MODELING THERMAL DEMAGNETIZATION AT THE LUNAR SWIRL REINER GAMMA. M. R. K. Seritan[1], I. Garrick-Bethell[1,2]. [1]University of California Santa Cruz, Santa Cruz, CA, USA. [2]School of Space Research, Kyung Hee University, Korea.

Introduction: The Moon no longer possesses a global magnetic field [1,2], but early in its history it had a dynamo that magnetized portions of the Moon's crust. We are able to measure the fields of these magnetic anomalies from orbit in the present day. There is no consensus on a formation mechanism for these magnetic anomalies, but investigating these them will allow us to place age and magnitude constraints on the Moon's thermal history [3,4] and perhaps on unusual dynamo generation mechanisms [5,6]. This work is an extension of previously presented work on Reiner Gamma, one of the Moon's strongest magnetic anomalies [7]. We extend the previous work with additional, more detailed modeling, that also suggests that portions of Reiner Gamma's morphology are due to thermal demagnetization from volcanic dome emplacement.

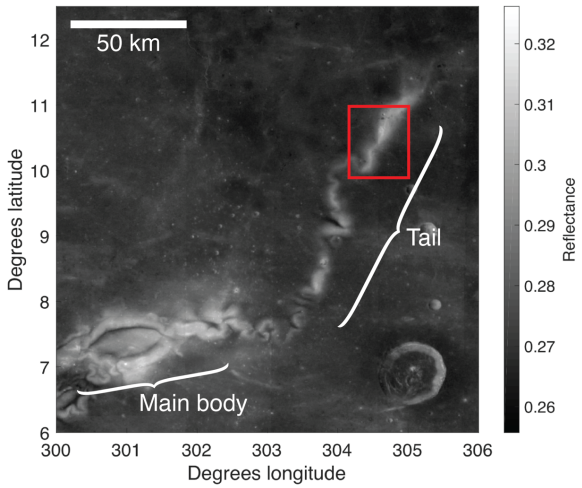

Fig. 1: A 750 nm Clementine reflectance image of Reiner Gamma with main body and tail indicated. The red box indicates the location of the dome in this work.

Reiner Gamma: The lunar swirl Reiner Gamma (Fig. 1) is located in Oceanus Procellarum and is collocated with some of the highest-magnitude magnetic anomalies on the Moon [8]. It can be divided into two parts: the elliptical 'main body' in the southwest, and the narrow and sinuous 'tail' that extends ~100 km to the northeast. The far northeastern end of the tail intersects the Marius Hills, a region with the highest density of volcanic domes on the Moon. Previous work has suggested that thermal demagnetization explains why the swirl does not overlay the centers of the nearby volcanic domes; the heat from the emplacement of the domes is what demagnetizes the swirl source bodies [7]. Swirl morphology changes on the order of millions of years [9], while the volcanism in this region ceased billions of years ago, so a change in swirl morphology is likely due to the swirl morphology itself changing, rather than being covered up by volcanism.

Modeling: To test the hypothesis of thermal demagnetization, we model this portion of Reiner Gamma in three sequential ways: (1) plate flexure modeling to determine the lateral extent and depth of the putative intrusion, (2) thermal modeling to determine the time-temperature history of the regions around the intrusion, and (3) magnetic source modeling to determine how demagnetization would manifest in the swirl's morphology.

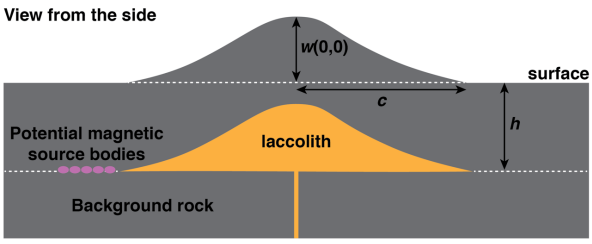

Fig. 2: The model laccolith labeled with the spatial parameters used in Equation 1. The semi-minor axis of the laccolith, *a*, is into the page. The potential source bodies of the swirl (left of the laccolith) are shown in purple at the same depth as the base of the laccolith.

Laccolith Modeling. We assume that the dome's topography is due to the intrusion of a lens-shaped body of magma, known as a laccolith [10] (Fig. 2). The reason for choosing this form is the close fit between an ideal laccolith shape and the north-south profile over the dome of interest. While the Marius Hills domes have a large extrusive component [11], our model assumes this particular dome to be completely intrusive. Hence, the results from this modeling process can be thought of as an upper bound for both burial depth and laccolith width. The vertical displacement, *w*, of a laccolith with an elliptical footprint can be represented by [10]:

$$w(x,y) = \frac{p_d}{8R} \frac{\left(1-\frac{x^2}{a^2}-\frac{y^2}{c^2}\right)^2}{\frac{3}{a^4}+\frac{3}{c^4}+\frac{2}{a^2c^2}} \quad (1)$$

where p_d is magma driving pressure, R is the flexural rigidity ($R = Eh^3/12(1-\nu^2)$, E is Young's modulus, h is the thickness of the overburden layer, and ν is Poisson's ratio), and a and c are the semi-minor and semi-major axes of the laccolith's elliptical footprint. Our model assumes p_d = 10 MPa [12,13], E = 25 GPa [14], ν = 0.25, and a/c = 7 km/8 km. The semi-major and semi-minor axes were chosen by locating the break in slope

between the dome's flank and the background plains, along the dome's the short and long axes. From this background topography level, we measured the maximum height of the dome, $w(0,0)$, to be 325 m. This value was inserted into Equation 1, and we solved for the overburden thickness h, yielding 870 m. For likely ranges of E and p_d, h can vary between ~700 m and ~1900 m.

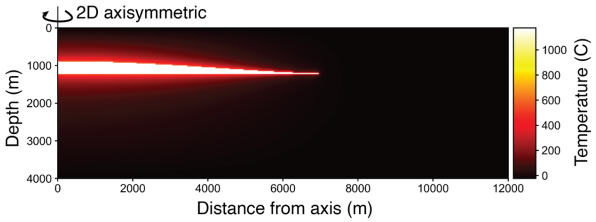

Fig. 3: The maximum temperature reached by each cell in 50,000 years.

Thermal Modeling. We created a 2D-axisymmetric model of the heat flowing away from the intruding laccolith. For this model, T_{hot} is 1175°C, T_{cool} is -23°C (the lunar mean near-surface temperature), and the liquidus and solidus of basalt were set to 1200°C and 1000°C, respectively. The release of 10^5 J/kg of latent heat [15] was distributed linearly between the liquidus and the solidus.

In this work, we assume that if the maximum temperature reached by a cell exceeds the Curie temperature of a magnetic carrier, then it will be completely demagnetized. We find that the demagnetization region around the intrusion does not extend more that ~100 m in the vertical direction and ~10 m in the horizontal direction (Fig. 3). These distances are very small compared to both the lateral extent of the laccolith and the overburden thickness. Thus, for the next stage of modeling, we assume that the intrusion must directly contact any swirl source bodies to induce thermal demagnetization.

Dipole Modeling. We forward-modeled the magnetic field produced by a 2D grid of equal-strength dipoles arranged to reflect the potential source body demagnetization suggested by the thermal modeling described above. First, we created a spatial distribution of dipoles that represents the swirl magnetic source bodies prior to any thermal demagnetization introduced by the intrusion of the laccolith. Next, we deleted dipoles according to which regions reached the Curie temperatures in the thermal model. We then calculated the magnetic field from the remaining dipoles (Fig. 4).

Results: We find that there are three features that occur in both the forward-modeled magnetic field and the observed swirl morphology: (1) a north-south strike in the region to the southwest of the local minimum, (box A in Fig. 4), (2) a local minimum along the path of the dipoles/swirl (box B in Fig. 4), and (3) field contours with a strike parallel to the northwestern edge of the dome (box C in Fig. 4). While the majority of the large-scale structure of the swirl may not be due to thermal demagnetization, these three common features support our thermal demagnetization model in this region. If this is indeed the case, we can constrain the burial depth of the swirl source bodies because, as per our thermal model, the thin edge of the laccolith must nearly intersect the swirl source bodies. A possible explanation for this coincidence would be if the source bodies were located on the same decollement surface on which the intrusion formed. This could be consistent with Reiner Gamma forming on top of pre-existing basalt during a temporary cessation of extrusive volcanism, until its subsequent burial [16], and finally partial thermal demagnetization through intrusive events. For the likely ranges of parameters used in Equation 1, the overburden thickness range from ~700 m to ~1900 m. This range of burial depths compares favorably to swirl source body depths as calculated in other works [17].

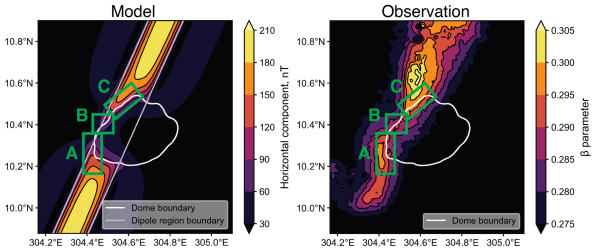

Fig. 4: A comparison between the modeled magnetic field (left, only horizontal component of the field shown) with the observed swirl morphology (right). The dome boundary (white contour) is defined by the -1420 m topography contour, which is the lowest closed topography contour around the dome. Green boxes denote similar morphologies, discussed below.

References: [1] Weiss, B. P. and Tikoo, S. M. (2014) *Science 346*, 1246753. [2] Tikoo, S. M. et al. (2017) *Sci. Adv. 3*, e1700207. [3] Stegman, D. R. et al. (2003) *Nature 421*, 143. [4] Zhang, N. et al. (2013) *JGR118*, 1789. [5] Dwyer, C. A. et al. (2011) *Nature* 479, 212. [6] LeBars, M. et al. (2011) *Nature* 479, 215. [7] Kelley, M. R. et al. (2018) *LPSC XLIX*, Abs. #2415. [8] Hood, L. L. and Schubert, G. (1980) *Science 208*, 49. [9] Hemingway, D. J. et al. (2015) *Icarus 261*, 66. [10] Pollard, D. D. and Johnson, A. M. (1973) *Tectonophysics18*, 311. [11] Weitz, C. M. and Head, J. W. (1999) *JGR 104*, 18933. [12] Wichmann, R. W. and Schultz, P. H. (1996) *Icarus 122*, 193. [13] Wöhler, C. and Lena, R. (2009) *Icarus 204*, 381. [14] Schultz, R. A. (1993) *JGR98*, 10883. [15] Barboza, S. A. and Bergantz, G. W. (1996) *Ro. Sci. Edin. 87*, 23. [16] Kelley, M. R. and Garrick-Bethell, I. (2020) *Icarus 338*, 113456. [17] Hemingway, D. J. and Tikoo, S. M. (2018) *JGR 123*, 2223.